Comparison between Parallel Hole and Rotating Slat Collimation with a Contrast Phantom using an Analytical Method

Lin Zhou, Kathleen Vunckx and Johan Nuyts

Abstract— **In this study, the parallel hole (PH) and the rotating slat (RS) collimators were compared based on a planar contrast phantom. Three figures of merit (FOMs) were applied for the comparison: the contrast-to-noise ratio (CNR) in a pixel of interest, the CNR in a region of interest, and the signal-to-noise ratio (SNR) of a channelized Hotelling observer (CHO). For the comparison purpose, all the FOMs were calculated analytically using an efficient approximation method.**

The comparison was mainly performed for planar imaging. The main results are: (1) By doing iterative reconstructions, it was verified that the analytical method can give accurate predictions for the proposed FOMs. (2) The gains (RS over PH) in all FOMs show the same tendencies in the system comparison. (3) PH only outperforms RS for cold spot imaging with a large phantom, while RS is better for all the other cases. (4) For system optimization, the optimal collimator apertures depend on the FOM to be optimized, however the ratio of the apertures (PH/RS) is always around $\sqrt{2}$, a value that we derived analytically in our previous work.

I. Introduction

One of the factors limiting the image quality in single photon emission computed tomography (SPECT) imaging is the trade-off between the spatial resolution and the geometric efficiency. For example, a conventional parallel hole (PH) collimator, which consists of a two-dimensional array of long narrow high-attenuating holes, only detects photons whose trajectories are almost parallel to these holes. Making these holes smaller will improve the spatial resolution, but at the same time decrease the geometrical efficiency significantly. For a reasonable spatial resolution, the geometric efficiency of a PH collimator is always very low. By contrast, a rotating slat (RS) collimator consists of a series of long thin septa which are positioned parallel with each other and perpendicular to the detector surface. This configuration allows in-plane photons collection, therefore a RS collimator can achieve a much higher geometric efficiency without any resolution loss. However, in order to interpret the plane integral data acquired by RS, even for planar imaging, an extra reconstruction step is needed, resulting in increased noise propagation.

It is not obvious whether or not a higher geometric efficiency obtained by the RS collimator will lead to improved image quality. In our previous work [1], the PH and the RS collimation systems were compared by investigating the contrast-to-noise ratio (CNR) of the central point of a homogeneous phantom using two analytical methods. However, SPECT imaging analysis often involves the investigation of a region of interest (ROI) or the detection of a hot/cold lesion. Therefore, in this study, we extended one of our analytical methods to evaluate the CNR in a ROI as well as the system performance in a lesion detectability task. Using different figures of merit (FOMs), the performance of PH and RS systems was compared at a fixed target resolution based on a contrast phantom.

Dept. of Nuclear Medicine, K.U.Leuven, B-3000 Leuven, Belgium.
This work is supported by F.W.O. grant G.0569.08. and I.U.A.P. grant NIMI.

II. Method

A. Theory

The analytical method that we used was first proposed by [2], [3] for converged maximum-a-posteriori (MAP) reconstruction. In our group it was adapted for post-smoothed maximum likelihood expectation maximization (MLEM) with a desired target resolution [4]. For a certain pixel j in the reconstruction image Λ, we define a set of filters:

$$Q_L^j = P^j G^j F^j \tag{1}$$

$$Q_C^j = P^j G^j F^j G^{jT} P^j \tag{2}$$

All the matrice are in $\mathbb{R}^{N\times N}$, with N the number of pixels in the reconstruction image. F^j is the approximated Fisher information matrix, G^j is the approximated pseudoinverse of F^j, P^j is an isotropic Gaussian post-smooth filter that tries to impose the given target resolution, and ^{T} denotes transpose. All factors are j-dependent due to the assumption of local shift-invariance [4].

For the chosen pixel j, the linearized local impulse response (LLIR) l_{pix} and the covariance image Cov_{pix} can be approximated as:

$$l_{\text{pix}}(\Lambda) \approx Q_L^j e^j \tag{3}$$

$$\text{Cov}_{\text{pix}}(\Lambda) \approx Q_C^j e^j \tag{4}$$

with e^j the j-th unit vector. The j-th elements of $l_{\text{pix}}(\Lambda)$ and $\text{Cov}_{\text{pix}}(\Lambda)$ are the contrast recovery coefficient (CRC) and the variance (VAR) in pixel j:

$$\text{CRC}_{\text{pix}} \approx e^{jT} Q_L^j e^j \tag{5}$$

$$\text{VAR}_{\text{pix}} \approx e^{jT} Q_C^j e^j \tag{6}$$

For a small uniform ROI centered at pixel j, we can write the vector of the ROI as:

$$R^j(i) = \begin{cases} 0 & \text{if } i \notin \text{ROI}, \\ 1 & \text{if } i \in \text{ROI} \end{cases} \tag{7}$$

with i the pixel index in the image space. The CRC and the variance of the mean value of this ROI are written as:

$$\text{CRC}_{\text{ROI}} \approx \frac{1}{N_R} R^{jT} Q_L^j R^j \tag{8}$$

$$\text{VAR}_{\text{ROI}} \approx \frac{1}{N_R^2} R^{jT} Q_C^j R^j \tag{9}$$

with N_R the total number of pixels in the ROI.

The CNR in a pixel or a ROI is defined as:

$$\text{CNR}_{\text{pix}} = \text{CRC}_{\text{pix}} / \sqrt{\text{VAR}_{\text{pix}}} \tag{10}$$

$$\text{CNR}_{\text{ROI}} = \text{CRC}_{\text{ROI}} / \sqrt{\text{VAR}_{\text{ROI}}} \tag{11}$$

For the lesion detectability, we used the signal-to-noise ratio (SNR) of a channelized Hotelling observer (CHO) as a figure of merit. SNR_{CHO} can be written as:

$$\text{SNR}_{\text{CHO}} = \sqrt{z^T U^T K^{-1} U z} \tag{12}$$

with z the ensemble mean difference of a reconstruction with and without the lesion, U the frequency-selective channels that mimic the human visual system, and K the covariance matrix of the channel output. For small lesions, we assumed that the presence of the lesion has negligible effect on the data. For a lesion located near pixel j, the approximations for z and K can be derived based on [4]–[7]:

$$z \approx Q_L^j \bar{f}_l \tag{13}$$

$$K \approx U Q_C^j U^T \tag{14}$$

with $\bar{f}_l$ the expectation of the lesion profile.

We compared the PH and the RS collimation systems by calculating the gain (RS over PH) in all three figures of merit (CNR_{pix}, CNR_{ROI} and SNR_{CHO}):

$$\text{Gain}_{\text{pix}} = \text{CNR}_{\text{pix}}^{\text{RS}} / \text{CNR}_{\text{pix}}^{\text{PH}} \tag{15}$$

$$\text{Gain}_{\text{ROI}} = \text{CNR}_{\text{ROI}}^{\text{RS}} / \text{CNR}_{\text{ROI}}^{\text{PH}} \tag{16}$$

$$\text{Gain}_{\text{CHO}} = \text{SNR}_{\text{CHO}}^{\text{RS}} / \text{SNR}_{\text{CHO}}^{\text{PH}} \tag{17}$$

With the definitions above, the tendencies of these gains as a function of different phantom parameters were investigated.

B. Validation

The analytical approximations in II-A (Eqs. (3)-(9), (13), (14)) can be validated by doing post-smoothed MLEM reconstructions. Given a certain pixel j, CRC_{pix}, CRC_{ROI} and z can be estimated from the reconstructions of the noiseless projection data of the phantom with and without an impulse, a ROI or a lesion located/centered at j. VAR_{pix}, VAR_{ROI} and K can be calculated from the reconstructions of a large number of noisy projection data sets.

Since the approximations of CNR_{pix} were already validated in [4], in this work we only verified for CNR_{ROI} and SNR_{CHO}. 100 noise realizations were simulated. The values of CNR_{ROI} and SNR_{CHO} calculated from the reconstructions were used as the reference values and compared with the values yielded by the analytical method.

C. Optimal Aperture

In [1], it was found that CNR_{pix} is influenced by the collimator aperture, and this influence differs from collimator to collimator. For a given target resolution and a certain collimator type, there exists an optimal collimator aperture which yields the maximal CNR_{pix} in the investigated pixel. In the framework of [1], we have only derived the optimal PH/RS aperture for CNR_{pix} as a function of the target resolution. However, different FOMs might yield different optimal collimator apertures. Therefore, following the same method as in [1], we calculated and compared the optimal PH/RS apertures which were optimized for CNR_{pix}, CNR_{ROI} and SNR_{CHO}, respectively.

D. Parameter Setting

The comparison between the PH and the RS collimator was mainly performed for planar imaging. For this purpose, a 128x128 detector array with detector size of 1.8x1.8mm^2 was modeled for both PH and RS. The image space was 128x128 with square pixels of 1.8mm. For RS there were 100 extra spinning angles equally distributed over 180 degrees. The distance between the phantom and the detector was 100mm. The full width at half maximum (FWHM) of the target resolution was fixed to 4 pixels. The septa heights of PH and RS collimator were optimized for CNR_{pix} at the given target resolution [1], resulting in 35.3mm and 50mm, respectively. The acquisition time was the same for both systems.

A planar contrast phantom is shown in Fig.1(a). The phantom consisted of an ellipse and two circles, representing the background (λ_b), the hot organ (λ_h) and the cold organ (λ_c), respectively. The ratio of the activity λ_h:λ_b:λ_c was 8:2:1, with λ_b=10^6 photons emitted per pixel in the total acquisition time. The pixels of interest were the central points of the two organs. Both the ROIs and the lesions were circular and located at the center of the organs. The ROIs had a diameter of 8 pixels and had the same activity as the organ, while the lesions had a diameter of 2 pixels and the lesion-to-organ contrast was 2.

For the calculation of SNR_{CHO}, we used a difference-of-Gaussians (DOG) model with 3 channels as the observer model. The channels were defined as the differences of pairs of a set of four 2-dimensional Gaussians. These Gaussians were with means of 0 and standard deviations of $(2d\sqrt{\pi})^{-1}$ where $d = 0.573, 0.995, 1.592$ and 2.653. These parameters were the same as in [8].

III. Result

A. Comparison of PH and RS

Using the phantom of Fig. 1(a), we calculated the gains in all three FOMs with various phantom settings. In each setting,

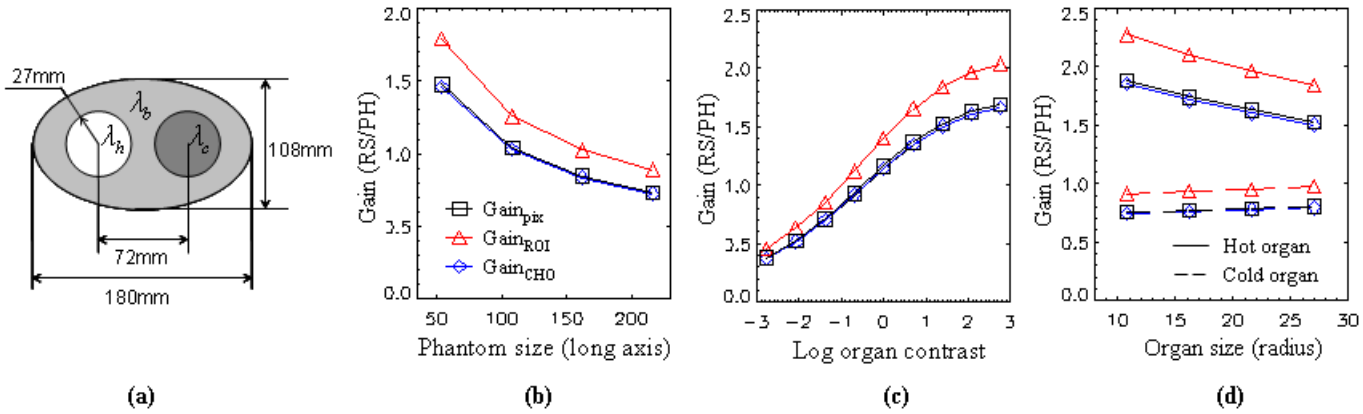

Fig. 1. (a) Contrast phantom. The ratio of activity $\lambda_h : \lambda_b : \lambda_c$ = 8:2:1. In the total acquisition time, $\lambda_b = 10^6$ photons emitted/pixel. (b)-(d) Gains (RS/PH) as a function of (b) phantom size, (c) organ contrast, (d) organ size.

we only changed one phantom parameter, and fixed all the other parameters to those indicated in Fig. 1(a). The comparison results are shown in Fig. 1(b)-(d), where the gains in CNR_{pix}, CNR_{ROI} and SNR_{CHO} are represented by the symbol of square, triangle and diamond, respectively.

1) Phantom Size: The phantom size was globally scaled by a factor of 0.3, 0.6, 0.9 and 1.2. Fig.1(b) shows the results in the cold organ. All the gains decrease with increasing phantom size.

2) Organ Contrast: In this setting, the contrast of the hot organ, i.e., λ_h/λ_b varies from 1/16 to 16. As shown in Fig.1(c), all the gains go up with increasing organ contrast. PH has better performance than RS in low contrast (cold) cases.

3) Organ Size: The sizes of both organs were simultaneously scaled by a factor of 0.4, 0.6, 0.8 and 1.0. Fig.1(d) shows that the all gains decrease with increasing organ size for the hot organ, while it is the opposite for the cold organ. Overall, RS is better in hot spot imaging (gains > 1) and PH has benefit in cold spot imaging (gains < 1).

B. Validation for CNR_{ROI} and SNR_{CHO}

The validation for CNR_{ROI} and SNR_{CHO} was done for each data point in III-A. The results are shown in Fig.2. The asterisk and triangle represent PH and RS, respectively. The approximated CNR_{ROI} (Fig.2(a)) and SNR_{CHO} (Fig.2(b)) are in good agreement with their corresponding reference values.

C. Optimal Aperture

Fig.3 gives the results about the optimal aperture. Here we still use the symbol of square/triangle/diamond to represent CNR_{pix}/CNR_{ROI}/SNR_{CHO}. The solid and dashed lines indicate PH and RS, respectively. As shown in Fig.3(a), each FOM yields its own optimal aperture sets. Although the optimal apertures are different for different FOM, the ratio of the optimal apertures (PH/RS) is always close to $\sqrt{2}$ (Fig.3(b)), a factor that we derived analytically in [1].

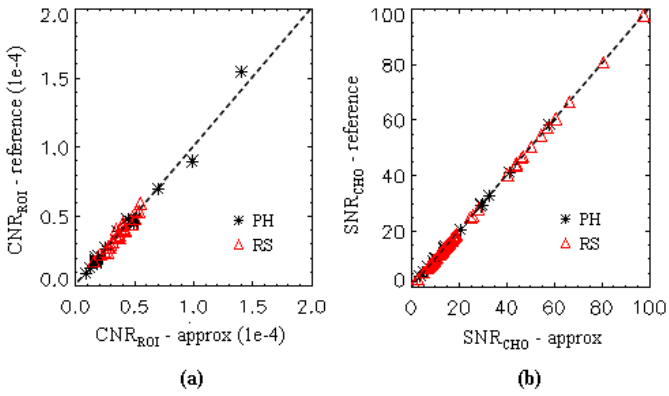

Fig. 2. The validation result of (a) CNR_{ROI}, (b) SNR_{CHO}. The dashed lines indicate the perfect agreement.

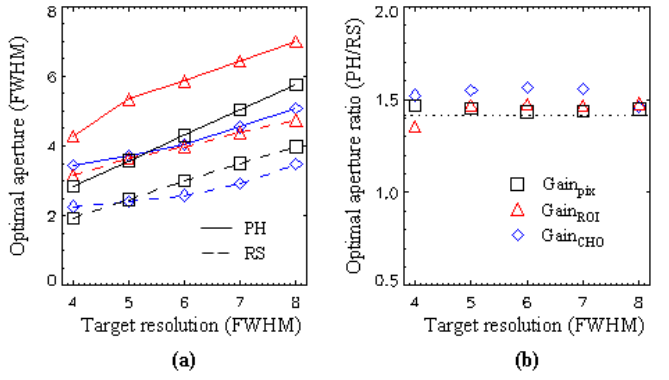

Fig. 3. (a) Optimal collimator apertures as function of the target resolution. (b) Ratio of the optimal aperture. The dashed line represents the value of $\sqrt{2}$.

IV. Discussion

In this work, the PH and the RS collimation systems were compared using three different FOMs (CNR_{pix}, CNR_{ROI} and SNR_{CHO}). In order to perform an efficient comparison, all the

FOMs were estimated by an adapted analytical method which predicts the image quality for the post-smoothed MLEM reconstruction. The validation results show that this method gives very accurate predictions for the purposed FOMs, therefore we trust this method and use it for the further investigation.

As shown in Fig.1, all these three FOMs give the same tendency in the system comparison. It means that when the phantom parameter varies, the relative performance of the two systems will be influenced in the same way for different imaging task, i.e., if one system is superior to the other system for the noise property in a ROI, probably it will also win in the aspect of lesion detectability.

Due to the increased noise propagation, RS always needs more post-smoothing than PH. Therefore, for a matched spatial resolution, the collimator aperture of RS should be smaller than that of PH. In our previous work [1], we found that the ratio of the collimator aperture (PH over RS) should be $\sqrt{2}$ when $\mathrm{CNR}_{\mathrm{pix}}$ is used as the FOM. Interestingly, as shown in Fig. 3, this rule remains valid for $\mathrm{CNR}_{\mathrm{ROI}}$ and $\mathrm{SNR}_{\mathrm{CHO}}$ as well. Based on this founding, we propose to compare PH and RS with their collimator aperture ratio equal to $\sqrt{2}$, no matter which figure of merit is under investigation.

The collimator apertures used in III-A were only optimized for $\mathrm{CNR}_{\mathrm{pix}}$. However, as long as the ratio of the apertures is close to $\sqrt{2}$, similar comparison results (as those shown in Fig. 1) will be obtained.

Based on the comparison results in Fig. 1, we can conclude that PH only wins for cold spot imaging combined with large background, while RS has better performance in all the other cases. Our conclusions are in good agreement with [9]. The difference between this work and [9] is that: 1) The two collimation systems were compared at equal spatial resolution in the final reconstruction. 2) The concept of the optimal aperture was applied. 3) Three different FOMs were estimated, representing the measurement for different investigation purposes.

Although this work is mainly focused on planar imaging, a preliminary experiment on volume imaging yields very similar results. Details are still under investigation.

V. Conclusion

We applied three FOMs ($\mathrm{CNR}_{\mathrm{pix}}$, $\mathrm{CNR}_{\mathrm{ROI}}$ and $\mathrm{SNR}_{\mathrm{CHO}}$) to compare the PH and the RS collimation based on a planar contrast phantom. The gains of all FOMs show the same tendencies in the system comparison. PH only outperforms RS for cold spot imaging with a large phantom, while RS is better for all the other cases. For system optimization, the optimal collimator apertures depend on the FOM to be optimized, however the ratio of the optimal aperture (PH/RS) is always around $\sqrt{2}$, a factor that we derived analytically in [1].

References

[1] L. Zhou, M. Defrise, K. Vunckx, and J. Nuyts, "Comparison between parallel hole and rotating slat collimation." *IEEE Nuclear Science Symposium Conference Record*, pp. 5530-5539, 2008.

[2] J. A. Fessler, "Mean and variance of implicitly defined biased estimators (such as penalized maximum likelihood): applications to tomography." *IEEE Trans. Image Processing.*, 5(3), pp. 493-506, 1996.

[3] J. Qi and R. M. Leahy, "A theoretical study of the contrast recovery and variance of MAP reconstructions from PET data." *IEEE Trans. Med. Imaging*, 18(4), pp. 293-305, 1999.

[4] K. Vunckx, D. Bequé, M. Defrise and J. Nuyts, "Single and multipinhole collimator design evaluation method for small animal SPECT." *IEEE Trans. Med. Imaging*, 27(1), pp. 36-46, 2008.

[5] J. Qi, "Analysis of lesion detectability in Bayesian emission reconstruction with nonstationary object variability." *IEEE Trans. Med. Imaging*, 23(3), pp. 321-329, 2004.

[6] A. Yendiki, J. A. Fessler, "Analysis of observer performance in known-location tasks for tomographic image reconstruction." *IEEE Trans. Med. Imaging*, 25(1), pp.28 41, 2006

[7] A. Yendiki, J. A. Fessler, "Analysis of observer performance in unknown-location tasks for tomographic image reconstruction." *J. Opt. Soc. Sm. A. Optic Image Sci. Vis.*, 24(12), pp. B99-B109, 2007

[8] H. C. Gifford, M. A. King, D. j. de Vries and E. J. Soares, "Channelized Hotelling and human observer correlation for lesion detection in hepatic SPECT imaging." *Journal of Nuclear Medicine*, 41(3), pp. 514-521, 2000.

[9] R. Van Holen, S. Vandenberghe, S. Staelens and I. Lemahieu, "Comparing planar image quality of rotating slat and parallel hole collimation: influence of system modeling." *Phys. Med. Biol.*, 53, pp. 1989-2002, 2008.